Silicon-Based Single-Mode On-Chip Ultracompact Microdisk Resonators With Standard Silicon Photonics Foundry Process

Weifeng Zhang, *Student Member, IEEE*, and Jianping Yao, *Fellow, IEEE, Fellow, OSA*

***Abstract*—A silicon-based on-chip ultracompact microdisk resonator (MDR) with a super-high Q-factor to support single-mode operation is designed, fabricated, and tested. In our design, a compact MDR has an ultrasmall radius of 3.7 μm with an additional slab waveguide incorporated to wrap the disk and the bus waveguide with an aim to weaken the disk sidewall roughness, to increase the confinement of the optical field and to strengthen the optical coupling between the bus waveguide and the disk. By using the three-level etching capability offered by a standard silicon photonics foundry, two ultracompact MDRs with two different heights of 220 and 150 nm are fabricated, in which the incorporated slab waveguide is kept to have an identical height of 60 nm. Optical performance of the MDRs is evaluated. The measured transmission spectrums show that both the MDRs are operating in single mode with no resonance splitting observed. The MDR with a height of 220 nm has a significantly improved Q-factor of 75,000, which is useful for narrowband filtering. The MDR with a height of 150 nm has a strong energy distribution around the top surface of the disk, which is useful for refractive index sensing. In addition, for the MDR with a height of 220 nm, owing to its ultrahigh light-confining capacity and ultracompact mode volume in the MDR, nonlinear optical response in the cavity is considerably enhanced and an optical bistability is observed experimentally when the input optical power is as small as −17 dBm.**

***Index Terms*—Microring resonator, microdisk resonator, optical bistability, silicon photonics.**

I. Introduction

SILICON photonics, a photonic integration platform, has attracted ever-increasing interest from the academia and industry for its compatibility with the current CMOS technology and its potential for seamless integration with electronic circuits [1], [2]. Intensive efforts have been devoted to developing various silicon photonic devices which could find applications in optical interconnects [3], low-cost telecommunications [4], microwave photonics [5] and biomedical engineering [6]. For future high-density and large-scale integrated photonic circuits, an individual device with a small footprint and a low power-consumption is highly needed, since it would elevate the integration density and power-efficiency of a chip.

Thanks to its small footprint and strong light-confining capacity, an on-chip optical micro-cavity is a key component in silicon photonic systems. Microring resonators (MRRs), as one common class of on-chip optical micro-cavity, have been extensively researched [7]. For example, an MRR can be used as a compact wavelength-selective filter in a wavelength-division multiplexing (WDM) network [8]. Incorporating a p-i-n junction in the waveguide, by using the free-carrier plasma dispersion effect in silicon, a high-speed electro-optic microring modulator has been demonstrated [9]. Moreover, an MRR can also be used as an optical delay line [10], a label-free bio-sensor [11], and a photonic microwave signal processor [12]. In addition, as a common class of on-chip optical micro-cavity, a microdisk resonator (MDR) exhibits advantages such as small footprint and high light-confining capacity [13]. Unlike an MRR that suffers from scattering loss caused due to sidewall roughness from both inner and outer sidewalls, an MDR experiences scattering loss only from the outer sidewall, thus the overall scattering loss is reduced and the Q-factor is increased. In addition, an MDR can have a much smaller radius. However, in contrast to the widespread applications of MRRs, few demonstrations have been reported to use MDRs for the aforementioned applications [8]–[12]. From the perspective of integration density, a smaller physical size of an individual device is always highly preferred. The main limitation hindering MDRs from widespread applications is the co-existing of multiple whispering-gallery modes (WGMs), since for most applications a single-mode operation over the entire free spectral range (FSR) is usually required. In addition, resonance-splitting as a result of Rayleigh scattering from the disk sidewall roughness would distort the spectral response, which would make it unsuitable for filtering applications. Furthermore, to make a high-speed microdisk modulator, it is required to incorporate a lateral PN junction in the MDR so that its resonant wavelength could be electrically tunable. However, since the first-order WGM supported by the disk is too close to the edge of the disk which gives an area that is not sufficiently large to make a lateral PN junction, it is extremely challenging to achieve a high-speed tunable MDR using the standard fabrication process. Although different approaches

Manuscript received April 6, 2017; revised July 5, 2017; accepted August 11, 2017. Date of publication August 14, 2017; date of current version September 8, 2017. This work was supported by the Natural Sciences and Engineering Research Council of Canada under the Silicon Electronic-Photonic Integrated Circuits CREATE program and the CMC Microsystems of Canada. *(Corresponding author: Jianping Yao.)*

The authors are with the Microwave Photonics Research Laboratory, School of Electrical Engineering and Computer Science, University of Ottawa, ON K1N 6N5, Canada (e-mail: wzhan088@uottawa.ca; jpyao@eecs.uOttawa.ca).

Color versions of one or more of the figures in this paper are available online at http://ieeexplore.ieee.org.

Digital Object Identifier 10.1109/JLT.2017.2740260

including a vertical PN junction [14] and a complicated disk structure [15] have been proposed, the large fabrication cost is an obstacle standing in the way for wide applications.

To circumvent these limitations, several designs have been proposed. A non-fully etched MDR with a radius as large as 20 μm has been demonstrated using a thin pedestal layer of silicon beneath the resonator to improve the Q-factor [16]. Thanks to the pedestal layer beneath the resonator, its unloaded Q-factor of the second-order WGM mode resonance is largely increased to 3×10^6. However, the MDR was fabricated using electron-beam lithography, which is not suitable for high-volume manufacturing because of its limited throughput. In addition, multiple WGMs co-exist and resonance splitting is observed, which is unwanted for most applications. By using a specifically-designed wrap-around bus waveguide, a planar silicon nitride MDR with a radius as large as 20 μm has been demonstrated to work in single mode [17], while the wrap-around bus waveguide design still requires an elaborate calculation to achieve the wrap-around angle.

In this paper, we report a silicon-based single-mode on-chip ultra-compact MDR fabricated with a standard silicon photonics foundry process. In the design, we add an additional slab waveguide to wrap the disk and the lateral sides of the bus waveguide, with an aim to weaken the disk sidewall roughness, to increase the confinement of the optical field and to strengthen the optical coupling between the bus waveguide and the disk. By making direct use of the three-level etching process offered by a standard silicon photonics foundry, two different MDRs with an identical radius as small as 3.7 μm and two different heights of 220 nm and 150 nm are fabricated. The slab waveguide in both MDRs is designed to keep an identical height of 60 nm. Optical performance of the MDRs is evaluated. By weakening the disk sidewall roughness impact on the confined optical field, the resonance-splitting problem is mitigated and the Q-factor is significantly improved. The measured transmission spectrums show that the MDRs are operating in single mode and no resonance-splitting is observed at a wavelength resolution of 2.4 pm. The MDR with a height of 220 nm has an improved Q-factor of 75,000, which is useful for filtering applications. In addition, the MDR with a height of 150 nm has a strong optical energy around the top surface of the disk, which is useful for refractive index sensing. Furthermore, owing to its ultra-high light-confining capacity and ultra-compact mode volume in the MDR with the height of 220 nm, nonlinear optical response in the cavity is considerably enhanced and an optical bistability is experimentally observed when the input optical power is as small as -17 dBm.

II. Design and Modelling

Fig. 1(a) illustrates the perspective view of three MDRs, in which Type-I disk is a conventional MDR, Type-II and Type-III disks are our proposed MDRs. To clearly illustrate the internal structure of the devices, the silica cladding layer is removed. Compared with the Type-I MDR, the distinct feature of our proposed Type-II MDR and Type-III MDR is that an additional slab waveguide is employed to wrap the disk and the lateral sides of the bus waveguide, which is able to weaken the impact

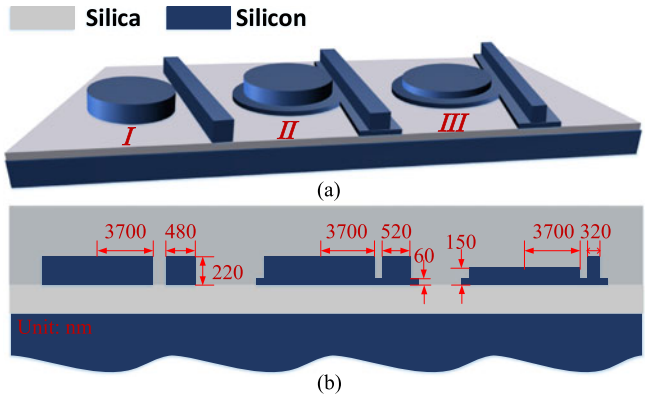

Fig. 1. (a) Perspective view of the three MDRs, (b) cross-sectional view of the three MDRs.

of the disk sidewall roughness on the confined optical field and to strengthen the optical coupling between the disk and the bus waveguide. To ease the design, the widths of the slab waveguide around the disk and the bus waveguide are kept identical, and in the coupling region the two slab waveguides are designed to fully overlap. Fig. 1(b) illustrates the cross-sectional view of the three corresponding MDRs. The three disks are designed to have an identical ultra-small radius of 3.7 μm and the coupling gap is chosen to be 180 nm. The widths of the slab waveguides are kept identical to the width of the coupling gap. For the Type-I MDR, the height of the disk is 220 nm; for the Type-II MDR the disk has a height of 220 nm and the slab waveguide has a height of 60 nm; for the Type-III MDR the disk has a height of 150 nm and the slab waveguide has a height of 60 nm. It is worth noting that the bus waveguides in the three MDRs have an identical height of 220 nm but different widths, which are specifically designed for each MDR to meet its phase-matching condition. Due to the multi-WGMs operation supported by an MDR, to effectively excite a specified WGM, the bus waveguide is designed to have a specific width to ensure that the effective refractive index of the TE mode supported by the bus waveguide is equal to the effective refractive index of the wanted WGM supported by the MDR [18]. In the MDR, the effective refractive index of the individual mode supported by the MDR can be calculated by

$$n_{\text{eff}} = \frac{m\lambda_0}{2\pi R} \tag{1}$$

where λ_0 is the resonance wavelength, m is azimuth harmonic number of the WGM, and R is the disk radius. After simulation using the finite difference time domain method (Lumerical FDTD Solutions), to effectively excite the first-order WGM in each MDR, the widths of the bus waveguide for the Type-I, Type-II and Type-III MDRs are determined to be 480, 520, and 320 nm, respectively.

Fig. 2 shows the energy profiles of the first-order and second-order radial TE modes supported by the MDRs with an identical radius of 3.7 μm. As can be seen from Fig. 2(a), the energy profile of the first-order radial TE mode supported by Type-I conventional MDR decays rapidly in the radial direction and outside the disk region, which indicates a weak optical coupling

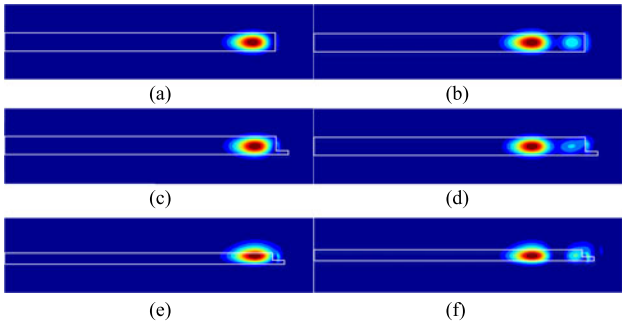

Fig. 2. The energy profiles of the (a) first-order and (b) second-order radial TE mode in the Type-I MDR; of the (c) first-order and (d) second-order radial TE mode in the Type-II MDR; and of the (e) first-order and (f) second-order radial TE mode in the Type-III MDR.

of the disk to a laterally adjacent bus waveguide. In order to make the MDR work in the critical coupling condition, such weak coupling often requires a very narrow coupling gap to increase the coupling strength, while the very narrow coupling gap would definitely increase the fabrication complexity. In addition, comparing with the second-order radial TE mode shown in Fig. 2(b), the first-order radial TE mode has a comparatively smaller mode volume and a strong electric field next to the sidewall, and hence exhibits higher sensitivity to the disk sidewall roughness, which finally results in a higher scattering loss and higher occurrence possibility of resonance-splitting. Fig. 2(c) and (d) shows the first-order and second-order radial TE modes supported by the Type-II MDR. Thanks to the slab waveguide, part of the sidewall is further away from the confined mode, which could weaken the impact of the sidewall roughness on the optical field due to optical scattering. In addition, the introduction of the slab waveguide would enable a strong optical coupling between the disk and the bus waveguide and hence it is much easier to achieve critical coupling while it is difficult in a conventional MDR. By choosing the bus waveguide width to make the first-order TE mode supported by the bus waveguide meet exactly the phase-matching condition for the first-order WGM supported by the MDR, the first-order WGM could be effectively excited in the disk thanks to the strong optical coupling, and the other higher-order WGMs could be effectively suppressed since the higher-order modes have a tendency to couple into leaky modes. Thus, a single-mode operation of the MDR is enabled. Fig. 2(e) and (f) shows the first-order and second-order radial TE modes supported by the Type-III MDR. It is clear to see that a lower height of the disk makes the supported TE modes have a much stronger energy around the top surface of the disk. Since the spectral positions of the resonances are strongly dependent on the refractive index contrast between the resonator and its surrounding environment, such a strong energy distribution around the top surface makes this MDR to have a high potential for refractive index sensing such as label-free bio-sensing [19]. Again, a much stronger energy tail of the second-order mode, as shown in Fig. 2(f), would have a tendency to couple the mode into a leaky mode to ensure a single-mode operation.

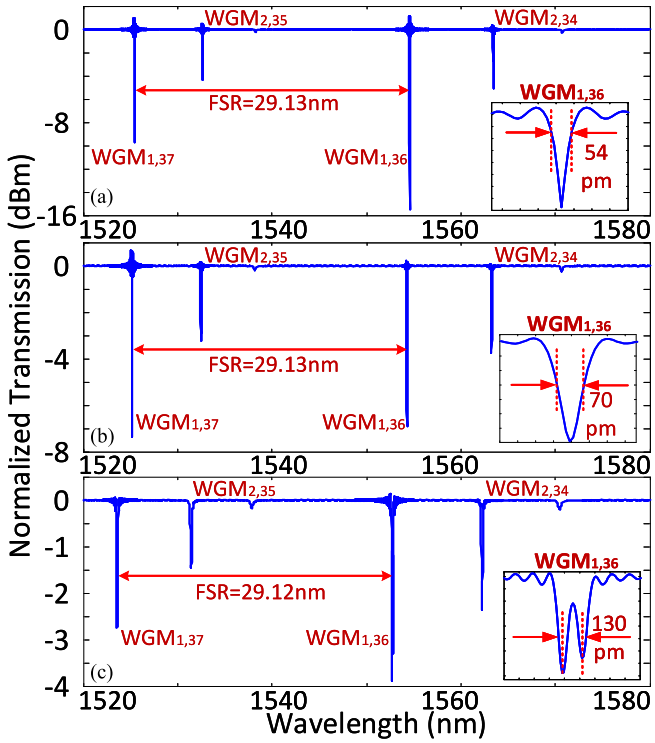

Fig. 3. Simulated transmission spectrums of the Type-I MDR with the magnitude of the sidewall roughness equal to (a) 0, (b) 10 and (c) 30 nm. The insets are the zoom-in views of the $\mathrm{WGM}_{1,36}$ mode resonance.

Due to fabrication imperfections, sidewall roughness always exists, which has a negative impact on the optical performance of an MDR due to the scattering of the confined optical waves. Firstly, a scattering loss is caused, which would largely increase the propagation loss of the confined light circulating in the disk and degrade the light-confining capacity of the disk. Secondly, the sidewall roughness scattering would also result in an optical coupling between the degenerate clockwise and counterclockwise traveling modes, which would cause unwanted resonance splitting [20], [21]. To verify the impact of the sidewall roughness on the optical performance, a simulation is made in a conventional MDR. In the simulation, the MDR has the same disk radius of 3.7 μm, bus waveguide width of 480 nm and coupling gap of 180 nm. Fig. 3 shows the simulated transmission spectrums of a conventional MDR when the disk sidewall roughness is gradually increased. The sidewall roughness is characterized statistically by the root-mean-square amplitude σ_r and the correlation length L_r. In the simulation, the correlation length L_r is set to be 20 nm while the amplitude of the roughness σ_r is gradually increased from 0 to 30 nm.

Fig. 3(a) shows the simulated transmission spectrum of the conventional MDR with zero roughness amplitude. Each notch in the spectrum represents a specific $\mathrm{WGM}_{\mathrm{p,q}}$ mode resonance in which p and q are the number of radial and azimuthal harmonic order, respectively. As can be seen, the first two orders of the WGMs are excited in the disk. The inset illustrates a zoom-in view of the $\mathrm{WGM}_{1,36}$ mode resonance which has a 3-dB bandwidth of 54 pm. Note that the transmission magnitude at the resonance wavelength is higher than 0 dBm, which is due

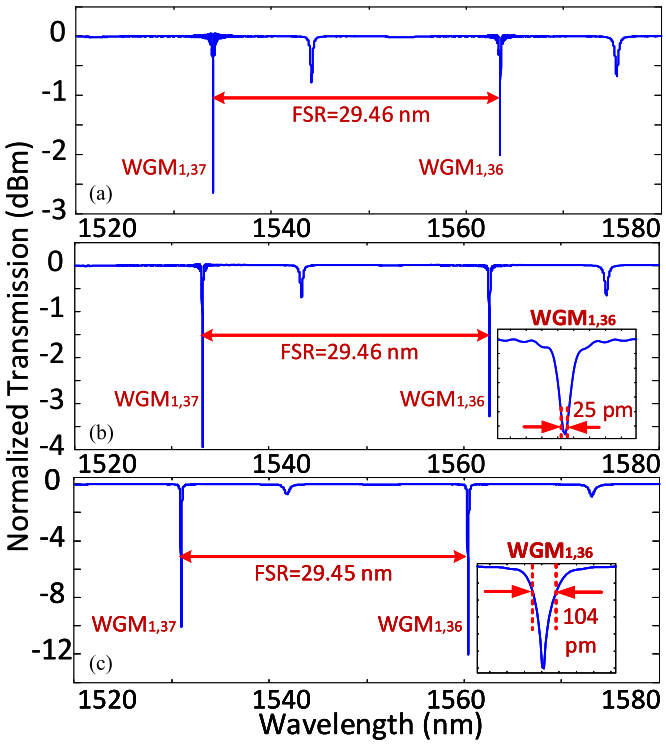

Fig. 4. Simulated transmission spectrums of the Type-II MDR with the magnitude of the sidewall roughness equal to (a) 0, (b) 10 and (c) 30 nm. The insets show the zoom-in views of the $\mathrm{WGM}_{1,36}$ mode resonance.

to the limited simulation time that causes the nonconvergence of the field at the resonance. When the roughness magnitude is increased to 10 nm, as shown in Fig. 3(b), again the first two orders of the WGMs are excited, while the 3-dB bandwidth of the $\mathrm{WGM}_{1,36}$ mode resonance is increased to 70 pm, which indicates a decrease in Q-factor of the disk. This is because a larger sidewall roughness would lead to a greater scattering loss for the confined optical field. When the roughness magnitude continues to be increased to 30 nm, the first two orders of the WGMs are still excited, and the 3-dB bandwidth of the $\mathrm{WGM}_{1,36}$ mode resonance is increased to 130 pm, which confirms again that a larger sidewall roughness would cause a greater scattering loss. More importantly, resonance-splitting happens, which is induced by optical coupling between the degenerate clockwise and counterclockwise traveling modes as a result of a strong sidewall roughness scattering. The resonance-splitting distorts the spectral response of the disk, which is unwanted for most applications and especially for filtering applications where a well-defined spectral response is needed. As the simulation results indicate, the large sidewall roughness results in a high scattering loss, which heavily degrades the optical-confining capacity of the MDR, and a high occurrence possibility of resonance-splitting would hinder it from a widespread application. However, owing to the fabrication imperfections, sidewall roughness is inevitable.

To verify the impact of the sidewall roughness on the optical performance of the Type-II MDR, a same simulation is performed except that the MDR has the Type-II configuration and a bus waveguide with a width of 520 nm is used. Fig. 4 shows the simulated transmission spectrums of the Type-II MDR with different sidewall roughness from 0 to 30 nm. As can be seen, as the sidewall roughness is increasing, the 3-dB bandwidth of the $\mathrm{WGM}_{1,36}$ mode resonance is increased, which indicates that the scattering loss caused by the sidewall roughness is increased with the sidewall roughness increasing. Due to the limited frequency resolution in the simulation, in Fig. 4(a) the extinction ratio of the $\mathrm{WGM}_{1,36}$ mode resonance is 2.0 dB. Compared with the simulation results of the Type-I MDR with the same sidewall roughness, the Type-II MDR presents a smaller 3-dB bandwidth of the $\mathrm{WGM}_{1,36}$ mode resonance, which verifies that the slab waveguide can weaken the sidewall roughness impact on the confined optical field since the additional slab waveguide makes part of the sidewall further away from the confined mode. In addition, as shown in Fig. 4, only the first-order WGM mode is effectively excited, which is distinct from the WGM mode excitation shown in Fig. 3, and no resonance-splitting is observed in Fig. 4. By making use of the three etching-level offered by a standard silicon photonics foundry, a slab waveguide could be made to wrap the disk and bus waveguide, which would increase the light-confining capacity of the optical cavity.

III. Fabrication and Characterization Results

To mitigate the impact of the sidewall roughness on the confined optical field, an additional slab waveguide is employed to wrap the disk and bus waveguide in the proposed Type-II and Type-III MDRs. The devices are designed to have an all-pass configuration and fabricated using a CMOS-compatible technology with 193-nm deep ultra-violet lithography in IMEC, Belgium. Note that three-level etchings are realized directly using the standard process and no other additional process is needed, which is of importance for mass production. Fig. 5(a) illustrates the SEM micrographs of the top-view of three fabricated MDRs, with all having an identical radius of 3.7 μm, which is much smaller than the radius of an MRR to be fabricated using the same process since such an MRR would have a very large bending loss. The ultra-compact footprint of the MDRs offers a compelling advantage in large-scale and high-density integration. Fig. 5(b) shows the sidewalls of the three MDRs captured at a sample tilt angle of 45°. The slab waveguide in the Type-II and Type-III MDRs has a height of 60 nm, and the disk in Type-III MDR has a height of 150 nm. Fig. 5(c) gives a closer view of the coupling region of the three MDRs.

The optical performance of the three MDRs is evaluated, which is done by measuring the transmission spectrums of the three fabricated MDRs using an optical vector analyzer (LUNA OVA CTe). Fig. 6(a) shows the normalized transmission spectrum of the fabricated Type-I MDR. As can be seen, the disk supports first-order and second-order WGMs, which matches well with the simulation result shown in Fig. 3 except a small resonance wavelength shift induced by the fabrication imperfections. The inset gives a zoom-in view of the $\mathrm{WGM}_{1,36}$ mode resonance. Resonance-splitting is observed, which is caused by Rayleigh scattering from the sidewall roughness. A 3-dB bandwidth of 105 pm is shown, corresponding to a normalized

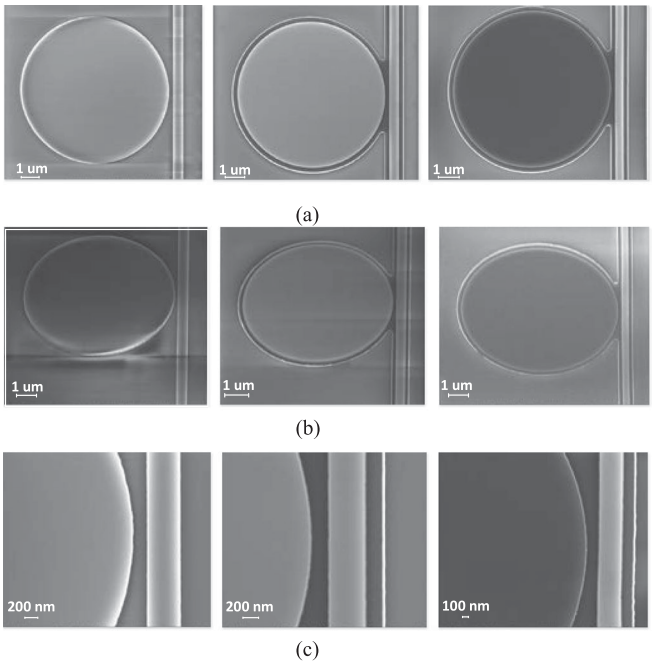

Fig. 5. (a) SEM micrographs of the fabricated three MDRs; (b) sidewalls of the three disks captured at a sample tilt angle of 45°; (c) a closer view of the structures at the coupling region.

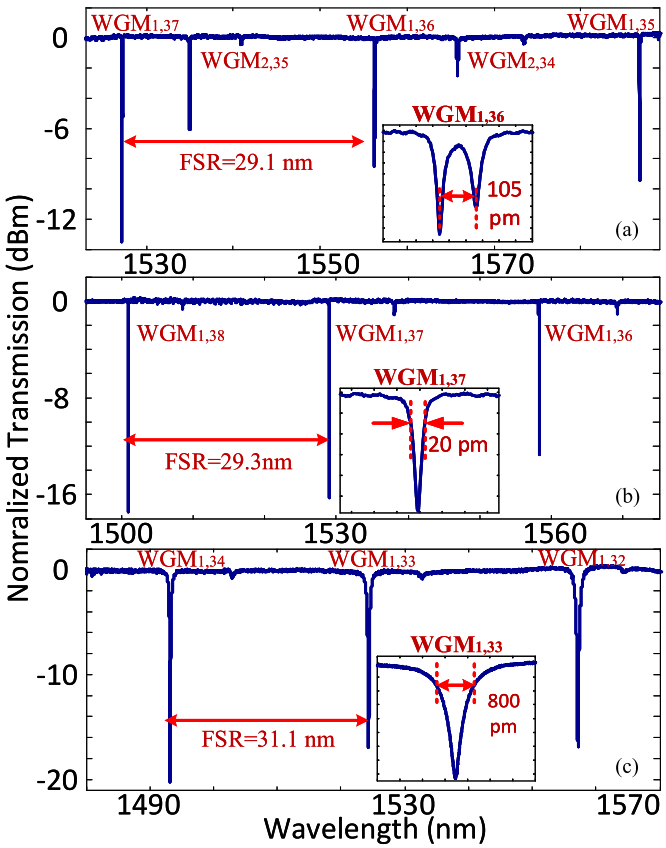

Fig. 6. Measured transmission spectrums of the fabricated (a) Type-I MDR, (b) Type-II MDR and (c) Type-III MDR. The insets show the zoom-in views of the $\mathrm{WGM}_{1,36}$ mode resonance for the Type-I MDR, $\mathrm{WGM}_{1,37}$ mode resonance for Type-II MDR, and the $\mathrm{WGM}_{1,33}$ mode resonance for the Type-III MDR.

splitting Q-factor of 15,600. Fig. 6(b) shows the normalized transmission spectrum of the fabricated Type-II MDR. The spectrum is clear and simple, only the first-order mode is supported and the high-order modes are effectively suppressed. This single-mode operation is resulted from the perfect phase matching in which the width of the bus waveguide is specifically designed to exactly excite the first-order mode in the disk, and the slab waveguide makes the high-order modes to couple into the leaky modes. In addition, no resonance-splitting is observed at a high resolution of 2.4 pm or 30 MHz. This is again attributed to the introduction of a slab waveguide surrounding the disk and the bus waveguide, which makes part of sidewall further away from the confined optical mode to weaken Rayleigh scattering from the sidewall roughness. The inset gives a zoom-in view of the $\mathrm{WGM}_{1,37}$ mode resonance, which has a 3-dB bandwidth of around 20 pm, corresponding to a Q-factor of 75,000. Compared with the Q-factor of the Type-I MDR, this Q-factor is significantly increased, which confirms a decreased scattering loss by using a slab waveguide. Note that the Q-factor of our proposed Type-II MDR is still smaller than the one reported in [16]. The main reason is that our proposed MDR has a much smaller radius of 3.7 μm than that in [16] which is as large as 20 μm. In addition, the Q-factor here is a loaded Q-factor calculated from the measured first-order WGM mode resonance, while in [16] the Q-factor is an unloaded Q-factor of the second-order WGM mode resonance, with the coupling loss not considered. The ultra-small size and super-high Q-factor is the distinct advantage of our proposed MDR. Furthermore, the introduction of a slab waveguide also creates the possibility for incorporation of a lateral PN junction to realize the electrical tunability. Fig. 6(c) shows the normalized transmission spectrum of the fabricated Type-III MDR. Again, a clear and simple spectrum is observed, which confirms again the effectiveness of our proposed design in enabling a single-mode operation and mitigating resonance splitting. The inset is a zoom-in view of the $\mathrm{WGM}_{1,33}$ mode resonance, which has a 3-dB bandwidth of around 800 pm, corresponding to a Q-factor of 2,000. The Q-factor is largely decreased due to the coupling loss caused by the different waveguide heights between the disk and the bus waveguide, and the increased radiation loss from the strong optical field near the disk top surface. From the measurement results, the MDR with a height of 220 nm has a significantly improved Q-factor, which is useful for narrowband filtering. The MDR with a height of 150 nm has a strong energy around the top surface of the disk, which is useful for refractive index sensing. Their ultra-compact features could elevate a high integration density and high power-efficiency of a chip.

IV. Optical Bistability

Thanks to its ultra-small footprint and super-high light-confining capacity of the Type-II MDR, a strong light-matter interaction would be enhanced in the micro-cavity. Particularly, its ultra-compact mode volume could largely reduce the optical power threshold required to generate optical bistability. Fig. 7 shows the transmission spectrum at the $\mathrm{WGM}_{1,36}$ mode

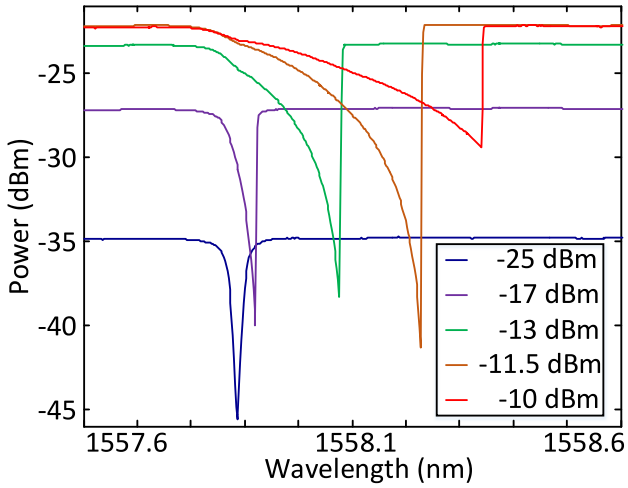

Fig. 7. (a) Measured transmission spectrum at the $\mathrm{WGM}_{1,36}$ mode resonance of the Type-II MDR for an optical wave with different power levels. Optical bistability is observed when an optical power is equal or above −17 dBm.

resonance when an optical wave with different powers is applied to the MDR. As can be seen, when the input optical power is equal or above −17 dBm, optical bistability occurs due to two-photon absorption induced nonlinear thermal-optic effect. To the best of our knowledge, this value is the lowest power ever reported so far. Note that in Fig. 7 only the upper arm of the bistable solution is shown, which is limited by our available measurement setup. The optical bistability with a required ultra-small optical power enables the MDR to operate as an optical switch, a logical gate, or an optical memory with an ultra-low power consumption [22].

V. Conclusion

We have reported a novel technique to design and implement a silicon-based on-chip ultra-compact MDR supporting single mode operation with a super-high Q-factor, which was realized by adding an additional slab waveguide to wrap the disk and the bus waveguide, and fabricated by a standard silicon photonics foundry. By making direct use of the three-level etching offered by a standard fabrication process, two different MDRs with an identical radius of 3.7 μm and two different heights of 220 nm and 150 nm, were fabricated. The optical performance of the two MDRs was evaluated and compared with a conventional MDR without an additional slab waveguide. The measured transmission spectrums showed that both the MDRs were operating in single mode with no resonance splitting being observed at a high wavelength resolution. For the MDR with a height of 220 nm, a significantly improved Q-factor of 75,000 was achieved. A MDR with a high Q-factor is suitable for wavelength filtering operation. For the MDR with a height of 150 nm, since the confined optical filed has a strong energy distribution around the top surface of the disk, and the spectral positions of the resonances are strongly dependent on the refractive index contrast between the MDR and its surrounding environment, this MDR held a great potential for refractive index sensing such as label-free bio-sensing. In addition, thanks to its ultra-small mode volume and super-high light-confining capacity of the Type-II MDR, optical bistability with ultra-small optical power consumption was experimentally studied. The key features of the proposed silicon-based on-chip MDRs include ultra-compact footprint, single-mode operation, no resonance splitting, and easiness for mass production, which make the proposed MDRs good candidates for applications in optical systems as optical switches, logical gates, and optical memories.

Acknowledgment

The authors would like to thank CMC Microsystems, for providing the design tools and enabling the fabrication of the device.

References

[1] M. Hochberg and T. B. Jones, "Towards a fabless silicon photonics," *Nature Photon.*, vol. 4, no. 8, pp. 492–494, Aug. 2010.
[2] B. Jalali and S. Fathpour, "Silicon photonics," *J. Lightw. Technol.*, vol. 24, no. 12, pp. 4600–4615, Dec. 2006.
[3] Z. Zhou, Z. Tu, T. Li, and X. Wang, "Silicon photonics for advanced optical interconnections," *J. Lightw. Technol.*, vol. 33, no. 4, pp. 928–933, Feb. 2015.
[4] M. Asghari and A. V. Krishnamoorthy, "Silicon photonics: Energy-efficient communication," *Nature Photon.*, vol. 5, no. 5, pp. 268–270, May 2011.
[5] W. Zhang and J. P. Yao, "Silicon-based integrated microwave photonics," *IEEE J. Quantum Electron.*, vol. 52, no. 1, Jan. 2016, Art. no. 0600412.
[6] Hu. X. Sun, A. Agarwal, and L. Kimerling, "Design guidelines for optical resonator biochemical sensors," *J. Opt. Soc. Amer. B*, vol. 26, no. 5, pp. 1032–1041, May 2009.
[7] W. Bogaerts *et al.*, "Silicon microring resonators," *Laser Photon. Rev.*, vol. 6, no. 1, pp. 47–73, Sep. 2011.
[8] F. Xia, M. J. Rooks, L. Sekaric, and Y. A. Vlasov, "Ultra-compact high order ring resonator filters using submicron silicon photonic wires for on-chip optical interconnects," *Opt. Express*, vol. 15, no. 19, pp. 11934–11941, Sep. 2007.
[9] Q. Xu, B. Shmidt, S. Pradhan, and M. Lipson, "Micrometer-scale silicon electro-optic modulator," *Nature*, vol. 435, no. 7040, pp. 325–327, May 2005.
[10] J. Cardenas *et al.*, "Wide-bandwidth continuously tunable optical delay line using silicon microring resonators," *Opt. Express*, vol. 18, no. 25, pp. 26525–26534, Dec. 2010.
[11] K. De Vos, I. Bartolozzi, E. Schacht, P. Bienstman, and R. Baets, "Silicon-on-insulator microring resonator for sensitive and label-free biosensing," *Opt. Express*, vol. 15, no. 12, pp. 7610–7615, Jun. 2007.
[12] W. Zhang and J. P. Yao, "Photonic generation of linearly chirped microwave waveforms using a silicon-based on-chip spectral shaper incorporating two linearly chirped waveguide Bragg gratings," *J. Lightw. Technol.*, vol. 33, no. 24, pp. 5047–5054, Dec. 2015.
[13] M. Soltani, Q. Li, S. Yegnanarayanan, and A. Adibi, "Toward ultimate miniaturization of high Q silicon traveling-wave microresonators," *Opt. Express*, vol. 18, no. 19, pp. 19541–19557, Sep. 2010.
[14] M. R. Watts, D. C. Trotter, R. W. Young, and A. L. Lentine, "Ultralow power silicon microdisk modulators and switches," in *Proc. IEEE 2008 Int. Meeting Group IV Photon.*, Sorrento, Italy, Sep. 2008, pp. 4–6.
[15] L. Zhou and A. W. Poon, "Silicon electro-optic modulators using p-i-n diodes embedded 10-microndiameter microdisk resonators," *Opt. Express*, vol. 14, no. 15, pp. 6851–6857, Jul. 2006.
[16] M. Soltani, S. Yegnanarayanan, and A. Adibi, "Ultra-high Q planar silicon microdisk resonators for chip-scale silicon photonics," *Opt. Express*, vol. 15, no. 8, pp. 4694–4704, Apr. 2007.
[17] E. Hosseini, S. Yegnanarayanan, A. Atabaki, M. Soltani, and A. Adibi, "Systematic design and fabrication of high-Q single-mode pulley-coupled planar silicon nitride microdisk resonators at visible wavelengths," *Opt. Express*, vol. 18, no. 3, pp. 2127–2136, Feb. 2010.
[18] M. Soltani, S. Yegnanarayanan, Q. Li, and A. Adibi, "Systematic engineering of waveguide-resonator coupling for silicon microring/microdisk/racetrack resonators: Theory and experiment," *IEEE J. Quantum Electron.*, vol. 46, no. 8, pp. 1158–1169, Aug. 2010.

[19] S. M. Grist *et al.*, "Silicon photonic micro-disk resonators for label-free biosensing," *Opt. Express*, vol. 21, no. 7, pp. 7994–8006, Apr. 2013.
[20] M. Borselli, T. J. Johnson, and O. Painter, "Beyond the Rayleigh scattering limit in high-Q silicon microdisks: Theory and experiment," *Opt. Express*, vol. 13, no. 5, pp. 1515–1530, Mar. 2005.
[21] M. Borselli, K. Srinivasan, P. E. Barclay, and O. Painter, "Rayleigh scattering, mode coupling, and optical loss in silicon microdisks," *Appl. Phys. Lett.*, vol. 85, no. 17, pp. 3693–3695, Oct. 2004.
[22] V. R. Almeida and M. Lipson, "Optical bistability on a silicon chip," *Opt. Lett.*, vol. 29, no. 20, pp. 2387–2389, Oct. 2004.

Weifeng Zhang (S'12) received the B.Eng. degree in electronic science and technology from Xi'an Jiaotong University, Xi'an, China, in 2008, and the M.A.Sc. degree in electrical engineering from the Politecnico di Torino, Torino, Italy, in 2011. He is currently working toward the Ph.D. degree in Microwave Photonics Research Laboratory, School of Electrical Engineering and Computer Science, University of Ottawa, Ottawa, ON, Canada.

His current research interests include silicon photonics and its applications in microwave photonics.

Jianping Yao (M'99–SM'01–F'12) received the Ph.D. degree in electrical engineering from the Université de Toulon et du Var, Toulon, France, in December 1997. He is a Distinguished University Professor and the University Research Chair in the School of Electrical Engineering and Computer Science, University of Ottawa, Ottawa, ON, Canada. From 1998 to 2001, he was with the School of Electrical and Electronic Engineering, Nanyang Technological University, Singapore, as an Assistant Professor. In December 2001, he joined the School of Electrical Engineering and Computer Science, University of Ottawa, as an Assistant Professor, where he became an Associate Professor in 2003, and a Full Professor in 2006. He became the University Research Chair in Microwave Photonics in 2007. In June 2016, he was conferred the title of Distinguished University Professor of the University of Ottawa. From July 2007 to June 2010 and July 2013 to June 2016, he served as the Director of the Ottawa-Carleton Institute for Electrical and Computer Engineering.

He has authored or coauthored more than 530 research papers (H-index: 58) including more than 320 papers in peer-reviewed journals and 210 papers in conference proceedings. He is a Topical Editor for *Optics Letters*, and serves on the Editorial Boards of the IEEE TRANSACTIONS ON MICROWAVE THEORY AND TECHNIQUES, *Optics Communications*, *Frontiers of Optoelectronics*, and *Science Bulletin*. He was as a guest co-editor for a Focus Issue on Microwave Photonics in *Optics Express* in 2013 and a Lead Editor for a Feature Issue on Microwave Photonics in *Photonics Research* in 2014. He currently serves as the Chair of the IEEE Photonics Ottawa Chapter and is the Technical Committee Chair of IEEE MTT-3 (Microwave Photonics). He has also served as the Chair for numerous international conferences, symposia, and workshops, including the Vice Technical Program Committee Chair of the IEEE Microwave Photonics Conference 2007, the TPC Co-Chair of the Asia-Pacific Microwave Photonics Conference 2009 and 2010, the TPC Chair of the high-speed and broadband wireless technologies subcommittee of the IEEE Radio Wireless Symposium 2009–2012, the TPC Chair of the microwave photonics subcommittee of the IEEE Photonics Society Annual Meeting 2009, the TPC Chair of the IEEE Microwave Photonics Conference 2010, the General Co-Chair of the IEEE Microwave Photonics Conference 2011, the TPC Co-Chair of the IEEE Microwave Photonics Conference 2014, and the General Co-Chair of the IEEE Microwave Photonics Conference 2015 and 2018. He has also served as a committee member for numerous international conferences, such as IPC, OFC, BGPP, and MWP. He received the 2005 International Creative Research Award of the University of Ottawa. He received the 2007 George S. Glinski Award for Excellence in Research. In 2008, he was awarded a Natural Sciences and Engineering Research Council of Canada Discovery Accelerator Supplements Award. He was selected to receive an inaugural OSA Outstanding Reviewer Award in 2012. He was an IEEE MTT-S Distinguished Microwave Lecturer for 2013–2015.

Prof. Yao is a registered Professional Engineer of Ontario. He is a Fellow the Optical Society of America and the Canadian Academy of Engineering.